
Article:
Turner, TD orcid.org/0000-0003-3776-2044, Nguyen, TTH, Nicholson, P et al. (4 more authors) (2019) A temperature-controlled single-crystal growth cell for the in situ measurement and analysis of face-specific growth rates. Journal of Applied Crystallography, 52 (Part 2). pp. 463-467. ISSN 0021-8898

https://doi.org/10.1107/S1600576719002048

JOURNAL OF APPLIED CRYSTALLOGRAPHY
ISSN 1600-5767

A temperature-controlled single-crystal growth cell for the *in situ* measurement and analysis of face-specific growth rates

T. D. Turner,[a]* T. T. H. Nguyen,[a] P. Nicholson,[b] G. Brown,[b] R. B. Hammond,[a] K. J. Roberts[a] and I. Marziano[c]

[a]Centre for the Digital Design of Drug Products, School of Chemical and Process Engineering, University of Leeds, Woodhouse Lane, Leeds, West Yorkshire LS2 9JT, UK, [b]School of Mechanical Engineering, University of Leeds, Leeds, West Yorkshire LS2 9JT, UK, and [c]Pfizer Worldwide Research and Development, Sandwich CT13 9NJ, UK. *Correspondence e-mail: t.d.turner@leeds.ac.uk

Received 15 August 2018
Accepted 5 February 2019

Edited by G. Renaud, CEA-Grenoble DSM/INAC/SP2M/NRS, Grenoble, France

Keywords: single-crystal growth measurement; crystal growth kinetics; single-crystal growth cell; crystal habit; habit modification.

Supporting information: this article has supporting information at journals.iucr.org/j

The design and construction of a growth cell for the precision measurement of face-specific single-crystal growth rates are presented. Accurate mechanical drawings in *SolidWorks* of the cell and individual components are provided, together with relevant construction models. A general methodology for its use in the measurement of single-crystal growth rates and their underpinning growth mechanism is presented and illustrated with representative data provided for the crystal growth of the {011} and {001} faces of *RS*-ibuprofen single crystals grown in ethanolic solutions. Analysis of these data highlights the utility of the methodology in morphological model development and crystallization process design.

1. Introduction

Crystallization is a key step in many industrial processes for the rapid isolation and selective purification of high-value compounds. One of the key stages of crystallization is the growth step of the crystalline particulates, which is reliant on certain conditions such as supersaturation, agitation, impurity content *etc*.; this ultimately defines the observed particle shape/habit. The particle shape is particularly important in downstream unit operations during processing of the material, in particular for filtration, drying, powder transfer/flow properties, tableting/compaction, blending *etc*. (Sun & Grant, 2001; Bansal *et al.*, 2007). Additionally, the particle shape determines surface properties/energy and hence has a large impact on the bioavailability/dissolution behaviour of active pharmaceutical ingredients (APIs), for example (Blagden *et al.*, 2007; Hammond *et al.*, 2007).

Much progress has been made in the area of crystal growth and habit prediction using both experimental and computational methodologies. Growth rate measurements of single crystals under diffusion-limited conditions at low driving force have been reported (Davey *et al.*, 1986; Davey & Mullin, 1974*a*,*b*; Cano *et al.*, 2001; Beckmann, 1986), and many studies have been conducted on populations of particles in agitated crystallizers to obtain mean crystal growth rate data (De Anda *et al.*, 2005; Li *et al.*, 2006; Rashid *et al.*, 2012; Ristić *et al.*, 1988). These methodologies (Van Driessche *et al.*, 2008) generally include the use of optical microscopy with phase contrast and/or polarized light, a recent example of which has been reported for the study of methyl stearate crystals, crystallized from various solution environments (Nguyen *et al.*, 2014; Camacho *et al.*, 2017; Toroz *et al.*, 2015).

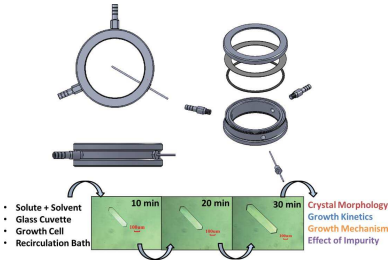

These examples highlight the utility of such measurements of face-specific growth rate data for both spontaneously nucleated and seeded crystals which provide the kinetic data to understand the impact of crystallization environment including solvent, supersaturation, impurity content *etc*. upon the habit of the final crystalline form. The baseline growth rate kinetic data can also be used to design crystallization processes which guide the material to a desired habit, whilst also avoiding crossing into certain growth regimes such as rough interfacial growth, where enhanced impurity uptake might be expected (Boistelle & Astier, 1988).

This communication presents the design of a temperature-controlled crystal growth cell and its associated construction diagrams, together with an outline methodology for its application in the measurement and analysis of face-specific growth rates of single crystals. This work details a useful workflow for the rapid and repeatable measurement of the crystal growth rate and kinetic data, which is illustrated through a case study example of *RS*-ibuprofen crystallizing from ethanolic solutions.

2. Single-crystal growth cell design

The single-crystal growth cell is shown in Fig. 1(*a*). It consists of a 0.5 ml, 54 × 10 × 1 mm borosilicate glass cuvette cell, which is held inside the main cell housing with a plastic cell holder. The main cell housing is constructed from stainless steel and consists of three components: 1 × main body assembly, 2 × end caps and 2 × nozzles. The stainless steel end caps screw onto the main body through 1 mm pitch threads. The main role of the end caps is to house the 2 × borosilicate glass windows (http://www.uqgoptics.com/), which allow image capture of the growing crystals within the cuvette and also act to keep the cell water tight. The cuvette cell is 1 ml in capacity and hence requires only small amounts of solute for experimental measurements. The plastic cap of the cuvette was modified by cutting one side flat so the cuvette can lie flat to improve image capture [a graphic to show a side view of the cell positioned on a microscope is provided in Fig. 1(*b*)]. The addition of the cuvette cell for the solute suspension is useful for reducing the amount of solute but also improves image capture, as the solution environment is stagnant yet still temperature controlled; this highlights a development on previous cells described in the literature (Jones & Larson, 1999). To achieve this the end caps contain glass cushions which are cut from a single piece of silicon and sit between the inside steel edge and the glass windows to prevent excessive application of pressure to the windows once screwed to the main body during use.

The main body assembly is machined from stainless steel; the top and bottom of the main cell body have machined 1 mm pitch threads onto which the end caps are secured. Additionally, the top and bottom of the main cell body contain O-ring grooves to house 2 × rubber O-rings. The sides of the main body contain 3 × tapped holes into which screw 2 × water bath nozzles and 1 × Pt100 housing plug. The nozzles allow connection of the cell to a water/oil circulator to vary the temperature of the cell contents. A detailed mechanical drawing of these components and how they are assembled is provided in Fig. 1(*c*). As can be seen from this drawing, the cell is simple in its design, resulting in improved ease of use and reduced time for experimental setup. Full mechanical drawings of the cell, a comprehensive list of peripheral components and a full mechanical description with dimensions of the components can be found in the supporting information together with `.SLDPRT` files (https://www.solidsolutions.co.uk/) for all the machined components.

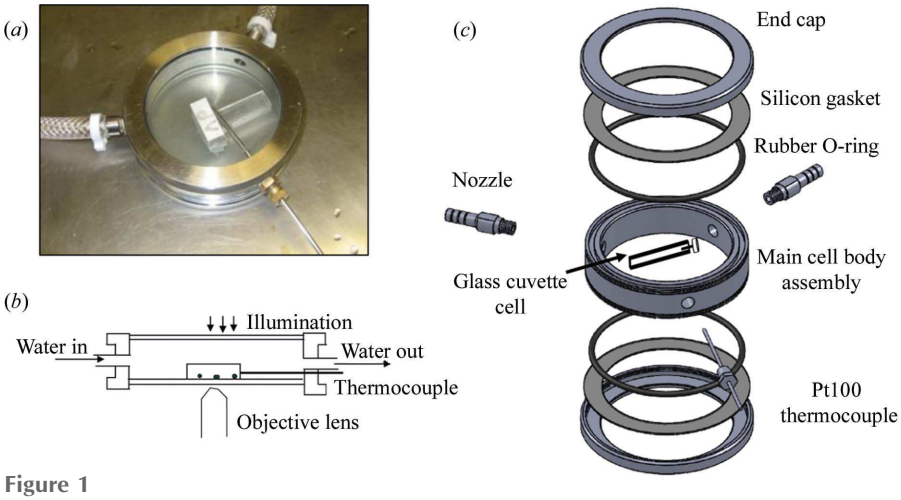

Figure 1
(*a*) Fully assembled growth cell showing the side nozzle connections to a water bath and a Pt100 thermocouple within the cell measuring the temperature around the sample cuvette cell [adapted from Nguyen *et al.* (2014) with permission from The Royal Society of Chemistry]. (*b*) Drawing of the cell in position on an inverted microscope (Nguyen, 2013). (*c*) Exploded mechanical drawing of the growth cell with the main components disassembled and highlighting the location of the cuvette cell.

3. Single-crystal growth rate measurements

A typical single-crystal growth measurement begins with preparation of a saturated solution of the solute of interest in the desired solvent. The solution is transferred to the 0.5 ml glass cuvette cell using a preheated syringe/pipette and sealed in with the plastic cap provided and laboratory film. The cuvette is transferred to the growth cell, which is then sealed and the temperature is set to achieve the desired supersaturation. Images of a nucleated single crystal are captured over the growth period at specific relative supersaturations, σ. σ is defined in equation (1), where c is the solution concentration, c^* is the equilibrium concentration and S is the supersaturation ratio:

$$\sigma = \frac{c - c^*}{c^*} = S - 1. \qquad (1)$$

An example of *RS*-ibuprofen single crystals grown from ethanol solutions at σ = 0.97, 0.79 and 0.66 is shown in Fig. 2.

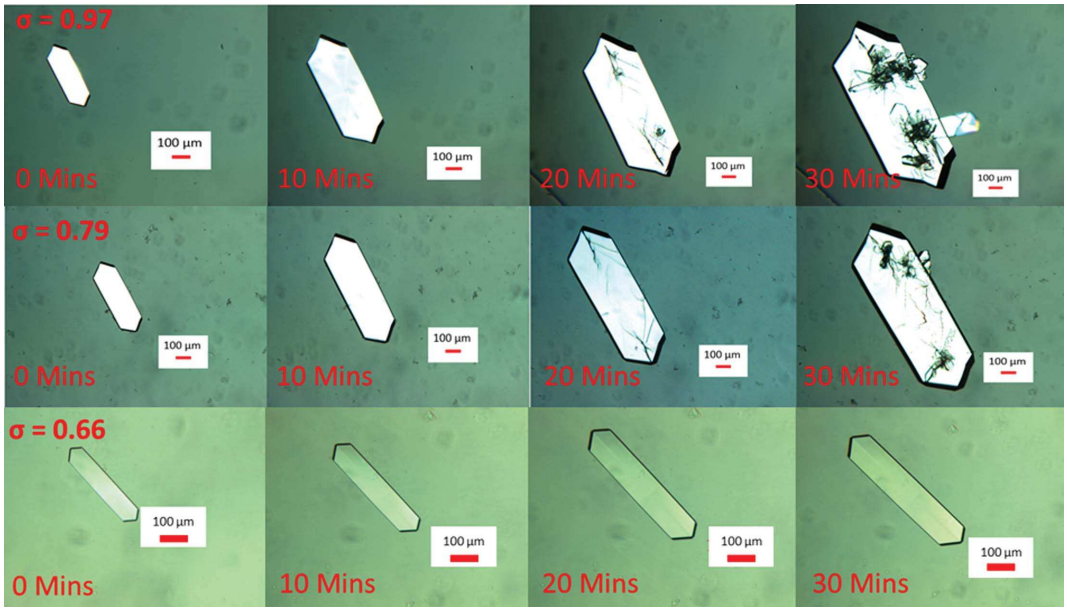

Figure 2
Example images from three single-crystal growth experiments of *RS*-ibuprofen grown from ethanol solutions at relative supersaturations 0.97 (top), 0.79 (middle) and 0.66 (bottom) [adapted from Nguyen *et al.* (2014) with permission from The Royal Society of Chemistry].

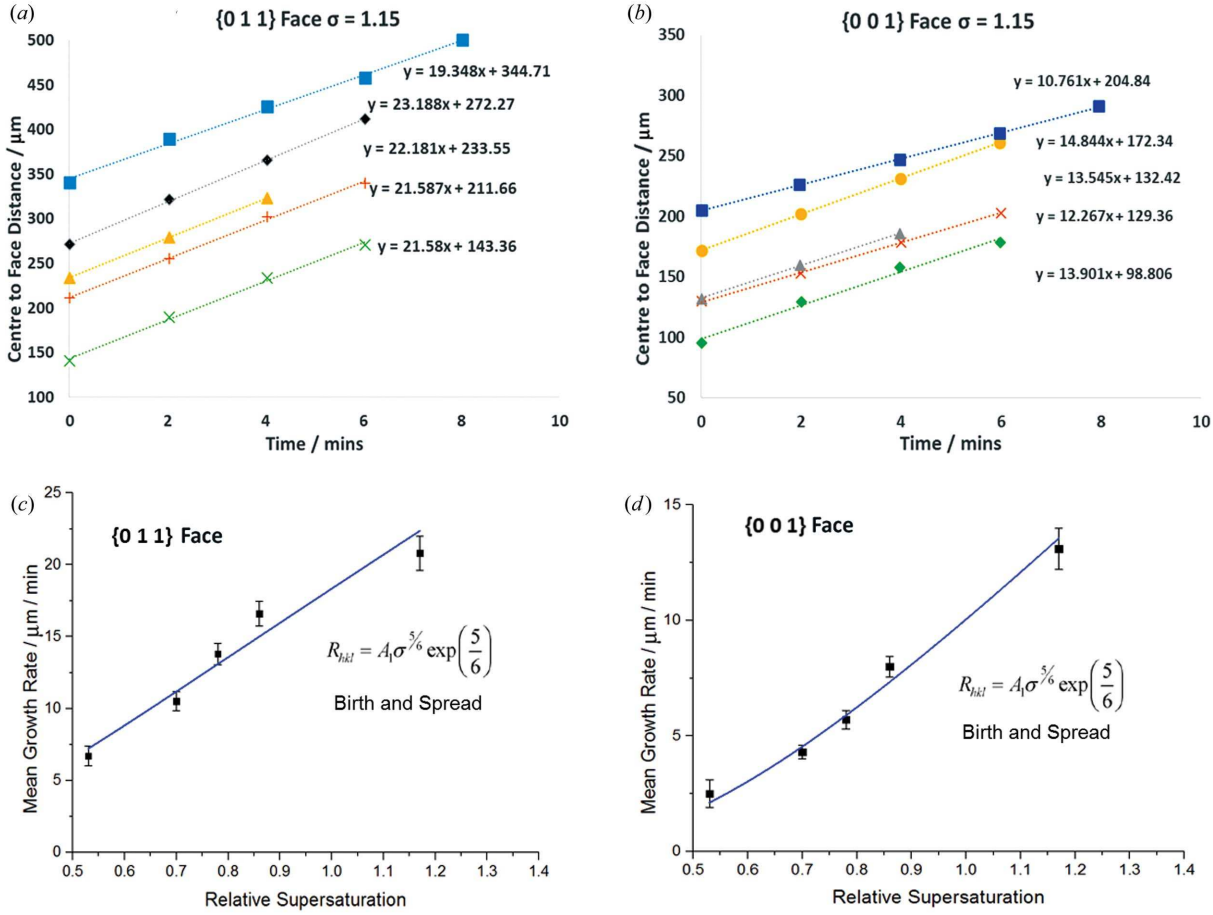

Figure 3
Crystal centre-to-face distances versus time plots for the (*a*) {011} and (*b*) {001} face of *RS*-ibuprofen at a relative supersaturation of 1.15, highlighting five experimental repetitions on new crystals; equations indicate the individual growth rates from the slope of the linear fit [adapted from Nguyen *et al.* (2014) with permission from The Royal Society of Chemistry]. Plot of the mean growth rate at five supersaturations for the (*c*) {011} and (*d*) {001} face of ibuprofen highlighting the fitting of the birth and spread model (Ohara & Reid, 1973; Eerden *et al.*, 1978) to the data [adapted from Nguyen *et al.* (2014) with permission from The Royal Society of Chemistry].

Additionally, a seeding crystallization process can be carried out, whereby the method is as described above, except that, at the holding temperature a single-crystal seed is quickly added into the cuvette cell.

The distance from the centre of the crystal to the crystallographic face is then measured from the micrographs. After repeating the measurement on new crystals, a mean growth rate, at the specified relative supersaturation, is determined. An example of this analysis is provided in Figs. 3(*a*) and 3(*b*), highlighting the calculated growth rates of the {011} and {001} faces, respectively, of five *RS*-ibuprofen single crystals grown from ethanolic solutions at σ = 1.15. The growth rates are calculated from the linear trends fitted to the centre-to-face distance versus time plots.

4. Assessing the growth mechanism

The average growth rates of the crystallographic faces of interest are measured over a range of supersaturations to provide an insight into the mechanism by which the crystal surfaces are growing. Three mechanisms are known for growth at crystalline *RS*-interfaces: rough interfacial growth (Bennema & Eerden, 1987; Dhanaraj *et al.*, 2010), birth and spread (Eerden *et al.*, 1978), and the Burton, Cabrera and Frank (BCF) screw dislocation model (Burton *et al.*, 1951); a more rigorous discussion of these three models is provided by Nguyen *et al.* (2014) and a further development into a two-step model is also provided by Camacho *et al.* (2017). Any of the above models or user-defined growth models can be used to assess the growth mechanism by means of a fitting process. The mean growth rates are plotted versus relative supersaturation, σ, which allows the various mechanistic models to be applied to the data. Figs. 3(*c*) and 3(*d*) show example data of mean growth rate versus σ plots from analysis of *RS*-ibuprofen crystals grown from ethanolic solutions. The various crystal growth models discussed above were then fitted to the data and a regression analysis was carried out to obtain the optimal fit to the data based on the value of R^2. In this case the birth and spread model was found to give the best fit to the data for both the {011} and {001} faces of *RS*-ibuprofen, indicating reasonably controlled growth at these faces. On assessing the growth mechanism it should be noted that a consequence of the cell geometry and the use of a cuvette cell is that the solution is stagnant and hence mass transfer could become rate limiting at a lower driving force. However, the benefit of this situation is that it provides a solution environment that is not affected by process factors such as stirrer speed, impeller geometry *etc.* and can provide 'baseline' growth kinetics for use in process development. This aspect could also be addressed by the user by application of micromagnetic stirring on the cell to provide solution agitation at a small scale.

5. Conclusions

This work highlights the utility of a single-crystal growth cell for the measurement of face-specific single-crystal growth rates in stagnant solutions. The developed growth cell design allows the simple efficient measurement of repeatable growth rate data and provides the benefit of a small sample cuvette, meaning less solute is required for multiple studies. Additionally, seeded and/or unseeded experiments can be carried out and the cell may also be used for dissolution experiments on nucleated single crystals. The data afforded using this technique allow routine determination of interfacial specific growth rates and mechanisms for the crystal system of interest and hence can be used for morphological model development. Further to this, the methodology presented could have industrial applications for improving crystallization process design to avoid impurity uptake and roughening transitions for a given crystallization system (Boistelle & Astier, 1988). Through its simplicity and small-scale size this cell provides a useful design tool for rapid screening studies when considering the impact of solvent, supersaturation, impurity content *etc.* on the morphology of crystalline materials.

Funding information

The authors gratefully acknowledge the financial support of this work by Pfizer and UK Northern Universities (N8) METRC initiative in molecular engineering. The authors also gratefully acknowledge the UK's Engineering and Physical Sciences Research Council (EPSRC) for the funding of crystallization research through a joint collaborative Critical Mass project (grant references EP/IO14446/1 and EP/IO13563/1). Morphological modelling work has been facilitated through the synthonic engineering project supported by EPSRC (EP/I 28293/1) in collaboration with a number of industrial companies.

References

Bansal, S. S., Kaushal, A. M. & Bansal, A. K. (2007). *Mol. Pharm.* **4**, 794–802.
Beckmann, W. (1986). *J. Phys. E Sci. Instrum.* **19**, 444–447.
Bennema, P. & van der Eerden, J. P. (1987). *Morphology of Crystals*, edited by I. Sunagawa, pp. 1–75. Tokyo: Terra Scientific.
Blagden, N., de Matas, M., Gavan, P. T. & York, P. (2007). *Adv. Drug Deliv. Rev.* **59**, 617–630.
Boistelle, R. & Astier, J. P. (1988). *J. Cryst. Growth*, **90**, 14–30.
Burton, W. K., Cabrera, N. & Frank, F. (1951). *Philos. Trans. R. Soc. A Math. Phys. Eng. Sci.* **243**, 299–358.
Camacho, D. M., Roberts, K. J., Muller, F., Thomas, D., More, I. & Lewtas, K. (2017). *Cryst. Growth Des.* **17**, 563–575.
Cano, H., Gabas, N. & Canselier, J. (2001). *J. Cryst. Growth*, **224**, 335–341.
Davey, R., Fila, W. & Garside, J. (1986). *J. Cryst. Growth*, **79**, 607–613.
Davey, R. & Mullin, J. (1974*a*). *J. Cryst. Growth*, **23**, 89–94.
Davey, R. & Mullin, J. (1974*b*). *J. Cryst. Growth*, **26**, 45–51.
De Anda, J. C., Wang, X., Lai, X., Roberts, K. J., Jennings, K., Wilkinson, M., Watson, D. & Roberts, D. (2005). *AIChE J.* **51**, 1406–1414.
Dhanaraj, G., Byrappa, K. & Prasad, V. (2010). *Springer Handbook of Crystal Growth*. Berlin, Heidelberg: Springer.
Eerden, J. P. van der, Bennema, P. & Cherepanova, T. (1978). *Prog. Cryst. Growth Charact.* **1**, 219–254.
Hammond, R. B., Pencheva, K., Roberts, K. J. & Auffret, T. (2007). *J. Pharm. Sci.* **96**, 1967–1973.
Jones, C. M. & Larson, M. A. (1999). *AIChE J.* **45**, 2128–2135.
Li, R., Thomson, G., White, G., Wang, X., De Anda, J. C. & Roberts, K. J. (2006). *AIChE J.* **52**, 2297–2305.

Nguyen, T. T. H. (2013). PhD thesis, School of Chemical and Process Engineering, University of Leeds, UK.
Nguyen, T. T. H., Hammond, R. B., Roberts, K. J., Marziano, I. & Nichols, G. (2014). *CrystEngComm*, **16**, 4568–4586.
Ohara, M. & Reid, R. C. (1973). *Modeling Crystal Growth Rates from Solution*, Vol. 225. Englewood Cliffs: Prentice-Hall.
Rashid, A., White, E., Howes, T., Litster, J. & Marziano, I. (2012). *Chem. Eng. Res. Des.* **90**, 158–161.
Ristić, R., Sherwood, J. N. & Wojciechowski, J. (1988). *J. Cryst. Growth*, **91**, 163–168.
Sun, C. & Grant, D. J. W. (2001). *J. Pharm. Sci.* **90**, 569–579.
Toroz, D., Rosbottom, I., Turner, T. D., Corzo, D. M. C., Hammond, R. B., Lai, X. & Roberts, K. J. (2015). *Faraday Discuss.* **179**, 79–114.
Van Driessche, A. E. S., Otálora, F., Sazaki, G., Sleutel, M., Tsukamoto, K. & Gavira, J. A. (2008). *Cryst. Growth Des.* **8**, 4316–4323.